ESP-JETA
ESP Journal of Engineering & Technology Advancements
ISSN: 2583-2646 / Volume 3 Issue 3 August 2023 / Page No: 15-22
Paper Id: JETA-V3I7P103 / Doi: 10.56472/25832646/JETA-V3I7P103

*Original Article*

# Aerodynamic Study of Minibus in Open and Closed Window Scenarios

**Olusola Oloruntoba[1], Oluwasanmi Alonge[2], Ojotu Joseph[3], Oluranti Abiola[4]**

[1,3,4]*Department of Automotive Engineering, Elizade University, Ilara-Mokin, Ondo State, Nigeria*
[2]*Department of Mechanical Engineering, Elizade University, Ilara-Mokin, Ondo State, Nigeria*

Received Date: 02 July 2023 Revised Date: 23 July 2023 Accepted Date: 05 August 2023

***Abstract:*** *Several vehicles in tropical Africa, such as Nigeria, operate with open window, and this is expected to affect aerodynamics of the vehicles. Based on established theory, Aerodynamic drag is a major component of energy losses which limit the energy available to propel a vehicle. The goal of this study is to determine the effect of open window on the aerodynamics of a typical minibus. ANSYS™ FLUENT™, a Computational Fluid Dynamics program, is applied to conduct numerical study in this work; vehicle speed is taken as 100km/h. Results from this study show that a characteristic chaotic flow in experienced in and around the vehicle with open window, leading to corresponding development of a chaotic turbulent flow on the frontal exterior region adjacent to frontal window, as well as the occurrence of a characteristic horse-shoe shaped flow which is formed on the outside of the wheels. These phenomena die out towards the rear of the vehicle trail. The corresponding characteristic turbulent flow is limited for closed window vehicle. Furthermore, aerodynamic drag and lift coefficients for closed window scenario are determined as 0.5773 and -0.1161 respectively; these values are 10.29% and 56.43% lower than the corresponding values for open window vehicle. The implications of the findings are: (a) higher aerodynamic drag leads to increase energy loss, fuel consumption and $CO_2$ emission, and (b) higher aerodynamic lift leads to reduced tire grip and increased instability, especially at corners.*

***Keywords:*** *Aerodynamics, Open Window, Closed Window, CFD, Drag, Lift*

## I. INTRODUCTION

Aerodynamic drag is a major component of energy losses which limit the energy available to propel a vehicle [1]–[3]. It can account for substantial part of the total energy losses at high speed regime [4], [5]. Several studies have shown that modification of vehicle shape can significantly increase or decrease energy loses due to aerodynamic drag [6]–[12]. Thus, careful study of the potential impacts of vehicle shape modifications on aerodynamics are required prior to implementations of the modifications. Although, these modifications are expected to conform to provisions made by vehicle manufacturers. An example of such modifications is the introduction of load carriage on vehicle roof. Another example of modifications to vehicle shape, which may have serious consequences of aerodynamics and drag losses as well as fuel consumption, is *open window*; several vehicles in tropical Africa, such as Nigeria, operate with *open window*. From technical standpoint, open window does not constitute structural modification of the vehicle. However, it does allow a reversible modification of vehicle shape. And as a result, the dynamics of air flow in and around the vehicle are expected to affect the dynamics of the vehicle. Hence, the goal of this work is to study the aerodynamics of air flow in and around a typical minibus under *open window* and *closed window* scenarios.

ANSYS™ FLUENT™, a well-established and Industry standard Computation Fluid Dynamics (CFD) Computer Program is used in this study.

## II. METHODOLOGY

### A. Vehicle Model

The vehicle model employed in this study is the Toyota™ HiAce™ 2020 model. Toyota™ HiAce™ is a common minibus for transportation such as in Nigeria. The geometric description of the Toyota™ HiAce™ minibus includes: overall length $(L) =$

This is an open access article under the CC BY-NC-ND license (https://creativecommons.org/licenses/by-nc-nd/2.0/)

$5.915\ m$, width $(W) = 1.950\ m$ and height $(H) = 1.990\ m$. Figure 1(a) shows a simplified geometry for the Toyota™ HiAce™ 2020 model with open window, while Figure 1(b) presents a corresponding illustration of the Toyota™ HiAce™ 2020 model with closed window.

**B. Open and Closed Window Configurations**

This study considers two window configurations, namely: (a) open window configuration, and (b) closed window configuration. The open window configuration, illustrated in Figure 1(a), consists of three open windows on either side of the Toyota™ HiAce™ minibus. Detailed dimensions adopted for the windows in this study are provided as shown in Figure 1(a). The closed window configuration is simply considered the absence of opening in the windows locations as sown in Figure 1(b).

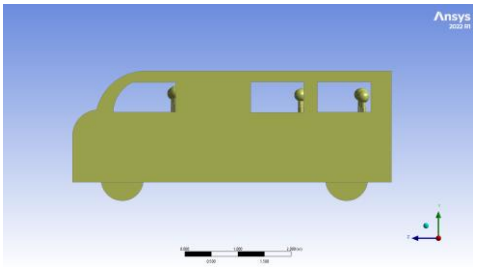


**(a) Open window configuration**

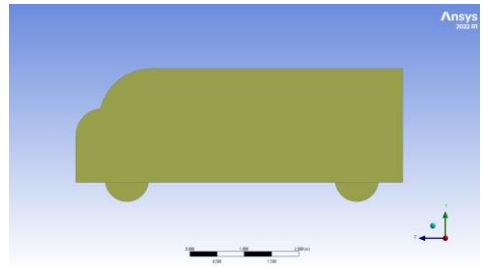


**(b) Closed window configuration**

**Figure 1: A simplified geometry for the TOYOTA™ HiAce™ minibus 2020 model**

**C. Numerical Window Tunnel Test Configuration**

The numerical experiments in this study are carried out in a numerical wind tunnel which is sufficiently large to realistically simulate aerodynamic flow of air in and around the Toyota™ HiAce™ 2020 model. The numerical wind tunnel is a modified version in the studies of [13] and [14], but an exact replica employed by [15]. Figure 2 shows the detailed geometric configuration of the numerical wind tunnel employed for this study.

$$\frac{\partial \rho}{\partial t} + \nabla \cdot (\rho \vec{v}) = 0 \qquad (1)$$

$$\frac{\partial (\rho \vec{v})}{\partial t} + \nabla \cdot (\rho \vec{v}\vec{v}) = -\nabla P + \nabla \cdot (\bar{\bar{\tau}}) + \rho \vec{g} \qquad (2)$$

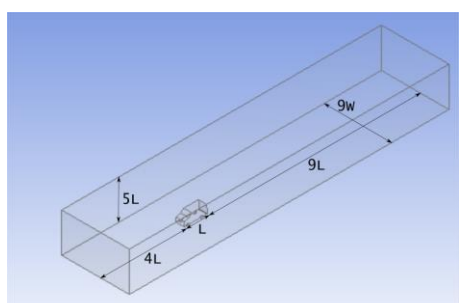


**Figure 2: Numerical wind tunnel and simplified TOYOTA™ HiAce™ minibus; dimension shown in terms of vehicle length (L) and width (W); (Source: (Oloruntoba and Okediji, 2021)).**

**D. Governing Equations and Boundary Conditions**

The applicable governing equations to study aerodynamic flow of air in and around the vehicle model in the numerical wind tunnel is the well-established Naiver-stoke equations [16], [17] which consists of three categories of equation, namely: conservation of mass, conservation of momentum and conservation of energy equations. In the study, variation in temperature is negligible, hence, conservation of energy equation is dropped. The set of conservation of mass and conservation of momentum equations to describe the flow in this study is given in Equations (1) and (2) respectively.

The symbols $\vec{v}$, $\rho$, $P$, $\bar{\bar{\tau}}$ and $\rho\vec{g}$ denote velocity vector of air flow, density of air, static pressure, stress tensor and gravitational body force respectively. Turbulent air flow of air in and around the vehicles is modelled using the SST $k-\omega$ viscous model [14], [18].

The boundary conditions of the numerical wind tunnel are specified pressure outlet and velocity inlet. The vehicle is stationary based on standard practice [9], the ground of the numerical wind tunnel is considered as a moving surface with same velocity as the inlet velocity. Thus, having the name relative velocity effect with a real-life scenario of moving vehicle on a stationary ground. Symmetry plane condition is applied to both the sidewalls and the roof of the numerical wind tunnel.

The inlet velocity is taken at a moderate speed 100 km/h for both cases considered in this study, namely: (a) open window and (b) closed window. The Reynolds number corresponding to (100 km/h) vehicle speed at vehicle length of 5.915 m is $Re = 11.25 \times 10^6$.

**E. Meshing, Simulation, and Coefficients of Lift and Drag**

Polyhedral mesh is applied in this study due to its high accuracy and speed. This advantage is attributed to the fact that each cell of the mesh is in contact with many other cells, leading to improved average estimate of flow parameter per cell and thus faster convergence [19]. Figures 3(a) and 3(b) show the polyhedral mesh for open window and closed window conditions of the TOYOTA™ HiAce™ minibus respectively.

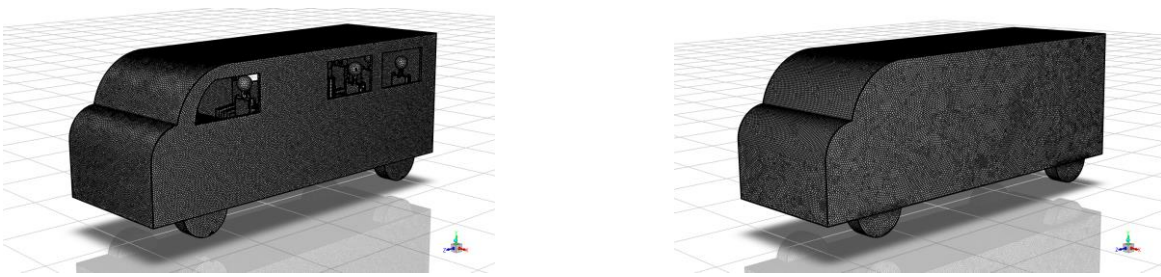

**(a) Open window configuration** **(b) Closed window configuration**

**Figure 3: Polyhedral mesh for the TOYOTA™ HiAce™ minibus 2020 model**

The final set of the governing equations described in Equations (1) and (2) are numerically discretized via the Finite Volume (FV) numerical scheme. Since the fluid flowing in and around the vehicle is air, the incompressible set of governing equations (i.e. Naiver-Stokes equation) are solved via the ANSYS™ FLUENT™'s Density-Based Solver. For simplicity, steady state flow scenario as well as absolute velocity are considered. Also, for realistic flow, turbulence is incorporated using the SST $k-\omega$ viscous model. Pressure-velocity coupling in the solution is achieved via the implicit solution method. The *Specific Dissipation Rate* used is the *First Order Upwind*. *Least Square Cell Based* and *Second Order Upwind* are applied for gradient and flow spatial discretization respectively.

Vehicle performance model is generally used to study road gradeability, maximum cruising speed of vehicle, and vehicle's acceleration and deceleration. As shown in equation (3), the transient vehicle performance model consists of five components.

$$F_P(t) = F_i(t) + F_d(t) + F_s(t) + F_R(t) \tag{3}$$

where, $F_P(t) =$ vehicle propulsion force, $F_i(t) =$ Inertia force of vehicle, $F_d(t) =$ total drag force of vehicle, $F_s(t) =$ Road slope resistance on vehicle, and $F_R(t) =$ Rolling Resistance of the vehicle's tires on the road.

For steady state condition ($F_i(t) = 0$), smooth surface or negligible rolling resistance ($F_R(t) = 0$), and uninclined road surface ($F_s(t) = 0$), Equation (3) simplifies to $F_P(t) = F_d(t)$. Thus, a detailed description of the simplified form of equation (3) is given in Equation (4). Where, $C_d =$ total drag coefficient (-), $F_d =$ total drag force (N), $A_F =$ vehicle frontal area (m$^2$), $\rho =$ density of air (kg/m$^3$), $v =$ vehicle velocity (m/s$^2$).

$$C_d = \frac{2F_d}{\rho A_F v^2} \qquad (4)$$

The dynamics of air flow in and around the bus results in a resultant Lift force on the vehicle, and the corresponding Lift coefficient is defined in Equation (5).

$$C_L = \frac{2F_L}{\rho A_L v^2} \qquad (5)$$

where, $C_L$ = lift coefficient (-), $F_L$ = lift force (N), $A_L$ = vehicle lift area (m$^2$), $\rho$ = density of air (kg/m$^3$), $v$ = vehicle velocity (m/s$^2$).

## III. RESULTS AND DISCUSSION

### A. Effect of Window Opening on Velocity and Pressure Profiles

Plan view velocity profiles of the Toyota™ HiAce™ minibus, subjected to velocity of 100 km/h (≡ 27.78 m/s), are given for both open and closed window scenarios in Figures 4(a) and 4(b) respectively. The highlights of the plots are as follows: first, for open window scenario, flow velocity appear to be lower (range: 0 - 13 m/s) around the front window in comparison with the closed window scenario; for closed window case the region with low velocity is much smaller. This indicates that, there is much lower retarded flow for closed window case. A similar observation was reported in a previous study where the velocity of air in the vehicle cabin is about 10% of the outer main stream [20]. In order to get a thorough understanding of this occurrence, vector plots superimposed on pressure profile are considered for both scenarios as shown in Figures 5(a) and 5(b) respectively.

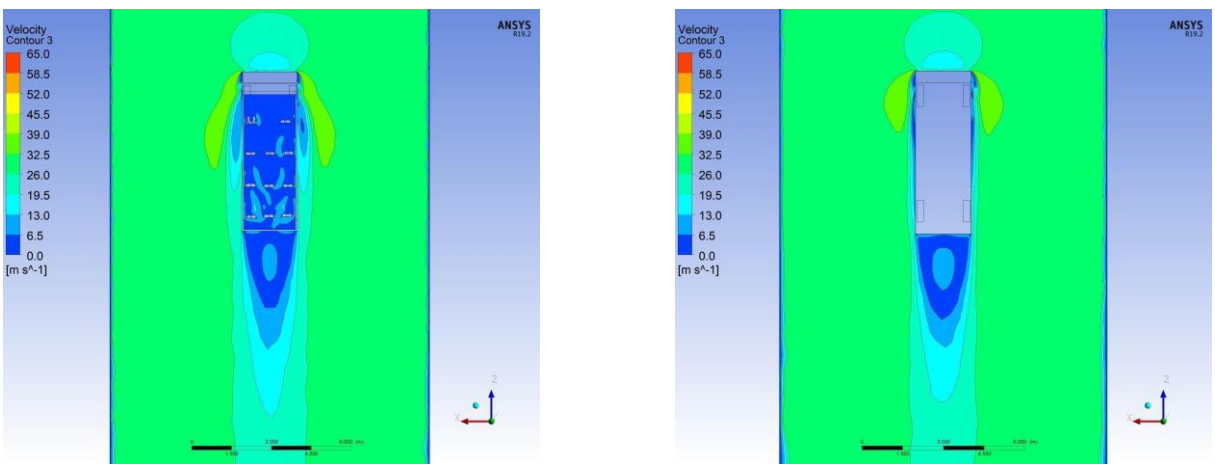


**(a) Open Window** **(b) Closed Window**

**Figure 4: Velocity contour for air flow around the TOYOTA™ HiAce™ minibus 2020 model**

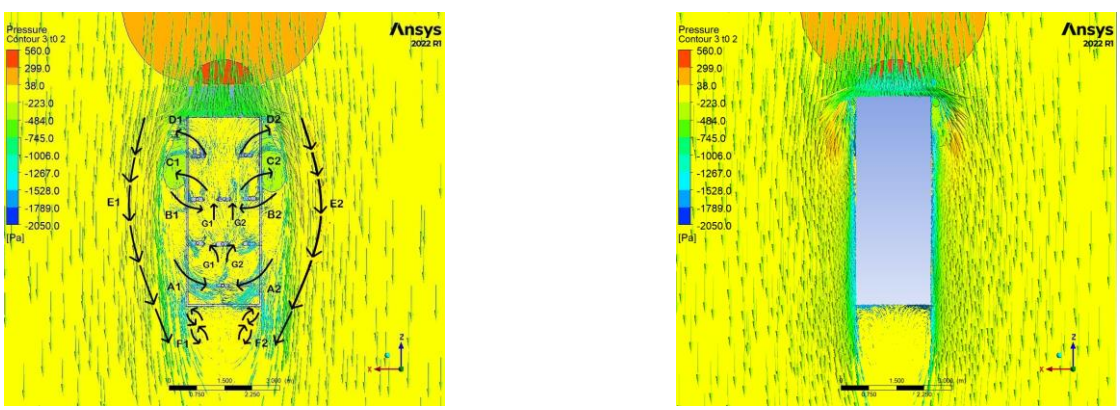


**(a) Open Window** **(b) Closed Window**

**Figure 5: Pressure profile for air flow around the TOYOTA™ HiAce™ minibus 2020 model**

For open window scenario, Figure 5(a) shows that air flowing against vehicle's frontal area divides into two streams, namely; stream *E1* and stream *E2*, and both streams, somewhat in part, flow round and towards the rear of the vehicle. Parts of

streams *E1* and *E2* enter the vehicle cabin via the rear windows as streams *A1* and *A2* respectively. Subsequently, streams *A1* and *A2* converge and flow towards cabin front as streams *G1* and *G2* respectively. At the middle windows, part of streams *G1* and *G2* exit the vehicle cabin as *C1* and *C2* respectively, while part of streams *E1* and *E2* enter the cabin as streams *B1* and *B2* respectively. Streams *C1* and *B1* form a cyclic flow on the left side of the vehicle, similar to streams *C2* and B2 on the right side of the vehicle. The remaining part of streams *G1* and *G2* proceeds further towards the front of the cabin where these streams transform into streams *D1* and *D2* respectively, and subsequently exit the cabin and commingle with streams *E1* and *E2* respectively. The observed flow pattern in this study corresponds to the findings of a previous study which recorded air flow inlet into a bus via the rear window and exits via front window [20]. The rationale behind the observations in this study as illustrated in Figure 5(a) is provided presently.

The flow of air against the frontal area of the vehicle is essentially due to vehicle velocity (100 km/h), leading to a build-up of air gauge pressure (≅357 Pa) at the vehicle's frontal area. The existence of lower pressure (<357 Pa) at locations that are above and beside the vehicle, causes this build-up of air to deflect towards the lower pressure regions. Taking a particular consideration of the side of the vehicle, as observed previously in this section, the rear windows experience air inflow into the cabin. This is due to the fact that the outside average gauge pressure (next to the rear window) at -75 Pa is higher than the inside average gauge pressure (next to the rear window) at -98.5 Pa, which follows directly from the Bernoulli's Principle. The front windows were also observed to exhibit one directional flow of stream, but out of the cabin. Pressure profile consideration is also applied, which demonstrates that the outside average gauge pressure (next to window) at -227.5 Pa is lower than the inside average pressure (next to window) at -174.5 Pa, thus justifying the outward flow of air from the vehicle cabin due to the Bernoulli's Principle. Bernoulli's Principle is also applied to explain the cyclic flow of air in and out of the middle windows. At the point of inflow into the cabin, outside average gauge pressure (next to window) is higher at -90 Pa compared to -160 Pa inside the cabin. Conversely at the point of outflow from the cabin, the outside average gauge pressure (next to window) is lower at -159 Pa compared to -141 Pa inside the cabin.

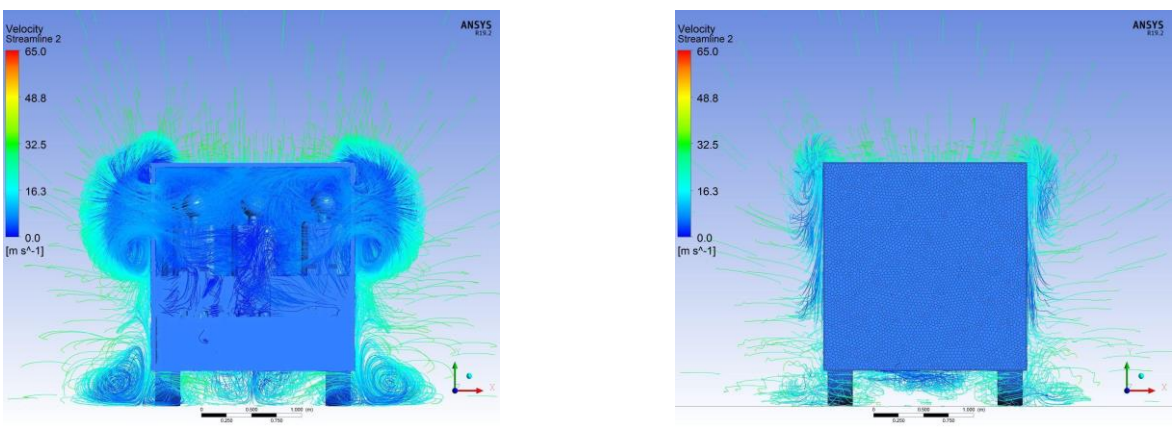


**(a) Open Window** **(b) Closed Window**

**Figure 6: Velocity streamline for air flow around the TOYOTA™ HiAce™ minibus 2020 model**

Figures 6(a) and 6(b) represent streamline plots for open and closed window scenarios of the Toyota™ HiAce™ minibus respectively. Based on the occurrence of air flow out of front windows as described previously, this outward flow (i.e. streams *D1* and *D2*) commingles with streams *E1* and *E2* respectively. Thus, resulting in a chaotic mixing region at low velocity (0 – 13 m/s) as shown in Figure 6(a). This characteristic mixing region is however absent for closed window, since streams *D1* and *D2* do not exist; only a minimal chaotic region exists. The chaotic or characteristic region would normally be examined from the point of view of turbulence, and thus this would be explored in detail later. Further consideration of Figures 6(a) and 6(b) reveals that the open window streamline plot exhibits a horseshoe-shaped flow characteristic on the outside of the wheel but non-existent for closed window scenario. A closer examination of Figure 6(a) suggests that the commingling of the air in the characteristic mixing region outside the front windows, setup a resultant horseshoe flow near the ground and on the outside of the wheels. This phenomenon is not present for closed window scenario, due to previously identified reason: the non-existence of streams *D1* and *D2*.

Figures 7(a) and 7(b) show the cross-sectional view of flow streamlines at -0.06 m behind the vehicle for open and closed window scenarios respectively. In both cases, a butterfly-shaped flow is exhibited, but it is more pronounced for open window case. This is due to the contributory air flow from vehicle cabin which commingles with air flow over and around the vehicle. The butterfly-shaped flow progressively reduces for both cases as observed in Figure 8(a) and 8(b) (i.e. for open and closed window scenarios) at location -1.5 m behind the vehicle. This reduced or damped behaviour is due to reduced cross flow between the main streams *E1* and *E2*, and the streams going in and out of the vehicle cabin, and thus resulting in situation where streams *E1* and *E2* predominantly influence the wake behind the vehicle.

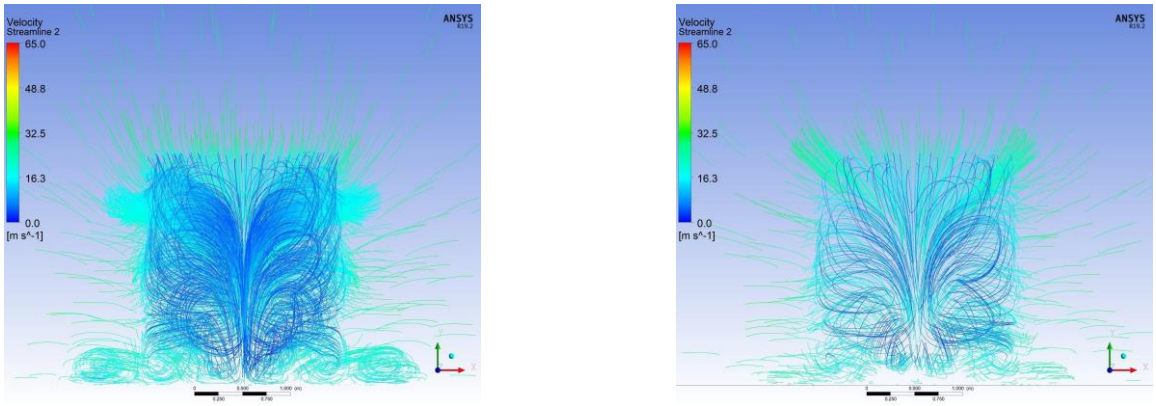


**(a) Open Window** **(b) Closed Window**

**Figure 7: Velocity streamline for air flow around the TOYOTA™ HiAce™ minibus 2020 model**

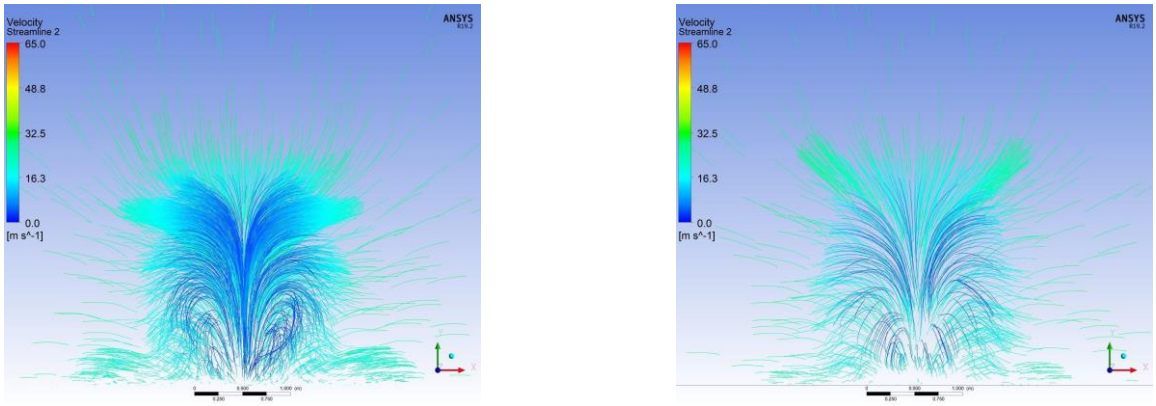


**(a) Open Window** **(b) Closed Window**

**Figure 8: Velocity streamline for air flow around the TOYOTA™ HiAce™ minibus 2020 model**

**B. Effect of Window Opening on Turbulence, Drag and Lift**

Figures 9(a) and 9(b) show velocity profile superimposed on vortices for open and closed window scenarios respectively, but with the vehicle body removed in order to allow clear visualisation of vehicle interior, especially for open window case. For both open and closed window scenarios, the vortices majorly developed from vehicle frontal region and near ground area owing to the commingling of streams *E1* and *D1* on the right side of the vehicle, and the commingling of streams *E2* and *D2* on the left side of the vehicle. The vortices are also due to the relative interaction between the chaotic mixing area (due to streams *E1* and *D1* as well as *E2* and *D2*) and the ground. These vortices progressively decay towards the rear of the vehicle due to damping effect of the open-air flow stream (over the vehicle). This damping, as described previously, is less effective for open window scenario due to the cross flow of air flow stream between the exterior and interior of the vehicle cabin. Also, the vehicle cabin experiences vortices essentially initialized from the rear window region and progressively envelopes the entire cabin, but at considerably lower velocity in comparison to vehicle exterior. This is attributed to constriction to air flow in the vehicle interior.

At the vehicle speed (i.e. 100km/h) considered in this study, aerodynamic drag coefficient $C_D$ for *closed window* scenario is 0.5773 while the corresponding value for *open window* scenario is 0.6367 (i.e. a 10.29% increase). This observation corresponds with the findings of a previous study which showed that window opening of a car in motion results in increase of aerodynamic drag [21]. This observation is majorly due to pressure drag introduced by air flow into the vehicle interior. The coefficient of lift $C_L$ for *closed window* scenarios is -0.1161 while the corresponding value for *open window* is -0.0506 (i.e. a 56.43% increase). A previous study also demonstrated that window opening of a bus has the effect of increasing both aerodynamic drag and lift [22]. As demonstrated in previous studies, an increase in $C_D$ leads to corresponding increase in $C_L$ [9].

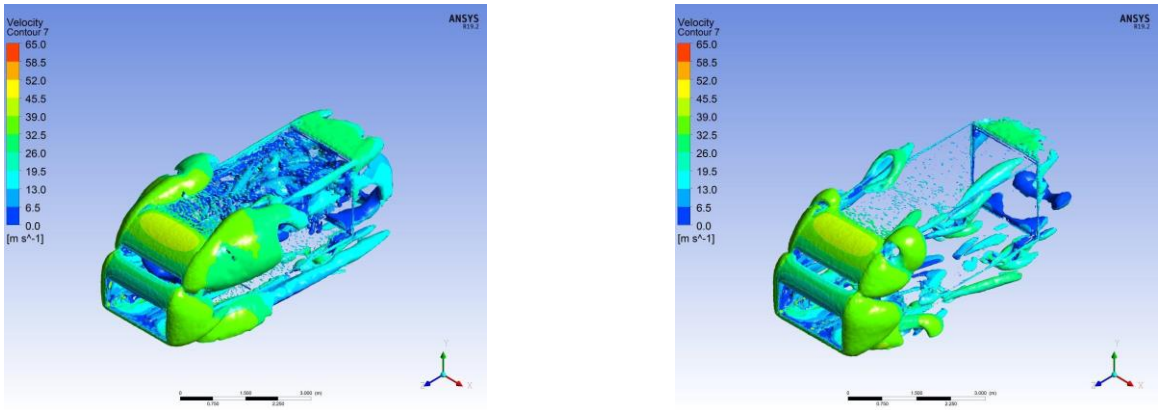


**(a) Open Window** **(b) Closed Window**

**Figure 9: Velocity contour superimposed on turbulent flow of air flow around the TOYOTA™ HiAce™ minibus 2020 model**

## IV. CONCLUSION

Aerodynamics of a TOYOTA™ HiAce™ minibus was studied in both *open* and *closed window* scenarios using ANSYS™ FLUENT™ Computational Fluid Dynamics (CFD) computer program. This study subjected the two scenarios of the vehicle to same identical numerical wind tunnel condition at vehicle speed of 100 km/h and standard environmental condition. The findings from the study include the followings.

First, *open* and *closed window* cases studied exhibited air flow over and around the vehicle. The *open window* however experienced inflow of air into the cabin through the rear window and outflow of air through the front window. The middle window experienced both inflow and outflow of air to form a cyclic flow. The occurrence of separated flow at the front of the vehicle contributed to reduced outer pressure adjacent to front window, when compared with the cabin interior and hence outflow of air; the reverse is the case at the rear of the vehicle. The middle window is a transition zone. This phenomenon on both sides, i.e. on the left and right sides, of the *open window* vehicle resulted in commingling of air as it flows in and towards frontal area of the cabin and diverging towards the right and left side of the cabin as it flows out of the front windows.

Also, a characteristic horse-shoe shaped flow is formed on the outside of the wheels for *open window* scenario due to commingling of air in the characteristic mixing region outside the front window. The horse-shoe shaped flow progressively dies out towards the rear of the vehicle due to reduced commingling of air in the rear mixing region.

Furthermore, chaotic turbulent flow is developed on the frontal exterior region adjacent to frontal window, and progressively dies out towards the rear of the vehicle due to damping effect of the open-air stream. The damping action is less effective for *open window* scenario owing to cross-flow of air between the interior and exterior of the vehicle cabin. Also, chaotic turbulent flow exists in the cabin interior but at lower velocity compared with the exterior vortices due to constricted flow in the cabin

Finally, aerodynamic drag and lift coefficients for *closed window* scenario are determined as 0.5773 and -0.1161 respectively. These values are 10.29% and 56.43% lower than the corresponding values for *open window* vehicle.

The implications of the findings are: (a) higher aerodynamic drags leads to increase energy loss, fuel consumption and $CO_2$ emission, and (b) reduced tire grip and increased instability, especially at corners.

## V. REFERENCES


[1] T. Q. Dinh, *Intelligent and Efficient Transport Systems - Design, Modelling, Control and Simulation*. 2020. doi: 10.5772/intechopen.81308.

[2] A. Eydgahi and E. L. Long, "Converting an Internal Combustion Engine Vehicle to an Electric Vehicle," presented at the 2011 ASEE Annual Conference & Exposition, Jun. 2011, p. 22.381.1-22.381.15. Accessed: Jan. 17, 2023. [Online]. Available: https://peer.asee.org/converting-an-internal-combustion-engine-vehicle-to-an-electric-vehicle

[3] S. Kaleg, A. Hapid, and M. R. Kurnia, "Electric Vehicle Conversion Based on Distance, Speed and Cost Requirements," *Energy Procedia*, vol. 68, pp. 446–454, Apr. 2015, doi: 10.1016/j.egypro.2015.03.276.

[4] C. Jux, A. Sciacchitano, and F. Scarano, "Tire dependence for the aerodynamics of yawed bicycle wheels," *J. Wind Eng. Ind. Aerodyn.*, vol. 233, p. 105294, Feb. 2023, doi: 10.1016/j.jweia.2022.105294.

[5] F. Malizia and B. Blocken, "Cyclist aerodynamics through time: Better, faster, stronger," *J. Wind Eng. Ind. Aerodyn.*, vol. 214, p. 104673, Jul. 2021, doi: 10.1016/j.jweia.2021.104673.

[6] A. P. Gaylard, N. Oettle, J. Gargoloff, and B. Duncan, "Evaluation of Non-Uniform Upstream Flow Effects on Vehicle Aerodynamics," *SAE Int.*, pp. 692–702, 2014, doi: 10.4271/2014-01-0614.

[7] G. L. Good, C. Johnson, B. Clough, and R. Lewis, "The Aesthetics of Low Drag Vehicles," *SAE Int.*, 2011, doi: 10.4271/2011-37-0016.

[8] J. Howell, K. Garry, and J. Holt, "The Aerodynamics of a Small Car Overtaking a Truck Tata Motors European Technical Centre," *SAE Int.*, 2014, doi: 10.4271/2014-01-0604.

[9] A. Huminic and G. Huminic, "Aerodynamic Study of a Generic Car Model with Wheels and Underbody Diffuser," *Int. J. Automot. Technol.*, vol. 18, no. 3, pp. 397–404, 2017, doi: 10.1007/s12239.

[10] M. I. Mukut and M. Z. Abedin, "Review on Aerodynamic Drag Reduction of Vehicles," *Int. J. Eng. Mater. Manuf.*, vol. 4, no. 1, pp. 1–14, 2019.

[11] T. Schuetz, *Aerodynamics of Road Vehicles*. Warrendale, Pennsylvania, USA: SAE International, 2016.

[12] M. Urquhart, M. Varney, S. Sebben, and M. Passmore, "Aerodynamic drag improvements on a square-back vehicle at yaw using a tapered cavity and asymmetric flaps," *Int. J. Heat Fluid Flow*, vol. 86, p. 108737, Dec. 2020, doi: 10.1016/j.ijheatfluidflow.2020.108737.

[13] N. Ashton and A. Revell, "Comparison of RANS and DES Methods for the DrivAer Automotive Body Comparison of RANS and DES Methods for the DrivAer Automotive Body," *SAE Int.*, 2015, doi: 10.4271/2015-01-1538.

[14] C. Zhang, C. P. Bounds, L. Foster, and M. Uddin, "Turbulence Modeling Effects on the CFD Predictions of Flow over a Detailed Full-Scale Sedan Vehicle," *Fluids*, vol. 4, no. 148, pp. 1–28, 2019, doi: 10.3390/fluids4030148.

[15] O. A. Oloruntoba and A. P. Okediji, "Effect of Speed and Boot Opening on Aerodynamics, Fuel Consumption, and CO2 Emission of Minibus," *FUOYE J. Eng. Technol.*, vol. 6, no. 4, Art. no. 4, Dec. 2021, doi: 10.46792/fuoyejet.v6i4.665.

[16] A. J. Chorin, "Numerical solutions of the Navier-Stokes equations," *Math Comput*, no. 22, pp. 745–762, 1968.

[17] J. Li, X. Lin, and Z. Chen, *Finite Volume Methods for the Incompressible Navier–Stokes Equations*. in SpringerBriefs in Applied Sciences and Technology. Cham: Springer International Publishing, 2022. doi: 10.1007/978-3-030-94636-4.

[18] ANSYS, *ANSYS FLUENT Theory Guide*, 17.0. Canonsburg, PA: ANSYS, Inc., 2016.

[19] M. Sosnowski, J. Krzywanski, K. Grabowska, and R. Gnatowska, "Polyhedral meshing in numerical analysis of conjugate heat transfer," vol. 02096, pp. 4–9, 2018.

[20] S. R. Kale, S. V. Veeravalli, H. D. Punekar, and M. M. Yelmule, "Air flow through a non-airconditioned bus with open windows," *Sadhana*, vol. 32, no. 4, pp. 347–363, Aug. 2007, doi: 10.1007/s12046-007-0029-3.

[21] J. S. M. Ali, S. M. Kashif, M. S. I. S. Dawood, and A. A. Omar, "Study on the effect of window opening on the drag characteristics of a car," *Int. J. Veh. Syst. Model. Test.*, vol. 9, no. 3–4, pp. 311–320, Jan. 2014, doi: 10.1504/IJVSMT.2014.066502.

[22] K. C. Nikam, L. D. Jathar, and S. L. Borse, "Study of Air Flow Through Non-Air-Conditioned Bus with Open Windows Using Open Foam," vol. 3, no. 7, pp. 105–120, 2015.


## AUTHORS BIBLIOGRAPHY


Olusola Oloruntoba, Lecturer, Elizade University (Ilara-Mokin, Nigeria)

Oluwasanmi Alonge, Lecturer, Elizade University (Ilara-Mokin, Nigeria)

Ojotu Ijiwo Joseph, Lecturer, Elizade University (Ilara-Mokin, Nigeria)

Oluranti Abiola, Senior Lecturer, Elizade University (Ilara-Mokin, Nigeria)